Received: 5 February 2025 | Revised: 10 April 2025 | Accepted: 28 April 2025

DOI: 10.1002/alz.70305

Alzheimer's & Dementia®
THE JOURNAL OF THE ALZHEIMER'S ASSOCIATION

RESEARCH ARTICLE

STING deletion protects against amyloid β–induced Alzheimer's disease pathogenesis

Jessica M. Thanos[1,2,3] | **Olivia C. Campbell**[1] | **Maureen N. Cowan**[1] | **Katherine R. Bruch**[4] | **Katelyn A. Moore**[1] | **Hannah E. Ennerfelt**[5] | **Nick R. Natale**[1,2] | **Aman Mangalmurti**[1,2] | **Nagaraj Kerur**[6,7,8] | **John R. Lukens**[1,2,3]

[1]Department of Neuroscience, Center for Brain Immunology and Glia (BIG), University of Virginia, Charlottesville, Virginia, USA

[2]Neuroscience Graduate Program, University of Virginia, Charlottesville, Virginia, USA

[3]Brain Immunology and Glia Graduate Training Program, University of Virginia, Charlottesville, Virginia, USA

[4]Department of Neurology, Massachusetts General Hospital, Boston, Massachusetts, USA

[5]Department of Neurology and Neurological Sciences, Stanford University, Palo Alto, California, USA

[6]Department of Ophthalmology and Visual Sciences, the Ohio State University Wexner Medical Center, Columbus, Ohio, USA

[7]Ohio State Havener Eye Institute, the Ohio State University Wexner Medical Center, Columbus, Ohio, USA

[8]Department of Microbial Infection and Immunity, the Ohio State University Wexner Medical Center, Columbus, Ohio, USA

Correspondence
John R. Lukens, Department of Neuroscience, Centre for Brain Immunology and Glia, University of Virginia, 409 Lane Road, MR4-6154, Charlottesville, VA 22908, USA.
Email: Jrl7n@virginia.edu

Funding information
National Institutes of Health, Grant/Award Numbers: R01AG071996, R01AG087406, RF1AG078684; National Institute of Neurological Disorders and Stroke, Grant/Award Number: T32NS115657; Harrison Family Foundation; Owens Family Foundation, Grant/Award Number: Grant; Cure Alzheimer's Fund, Grant/Award Number: Grant; Alzheimer's Association, Grant/Award Number: ADSF-21-816651; National Institute on Aging, Grant/Award Number: RF1AG078684

Abstract

INTRODUCTION: While immune dysfunction has been increasingly linked to Alzheimer's disease (AD) progression, many major innate immune signaling molecules have yet to be explored in AD pathogenesis using genetic targeting approaches.

METHODS: To investigate a role for the key innate immune adaptor molecule, stimulator of interferon genes (STING), in AD, we deleted *Sting1* in the 5xFAD mouse model of AD-related amyloidosis and evaluated the effects on pathology, neuroinflammation, gene expression, and cognition.

RESULTS: Genetic ablation of STING in 5xFAD mice led to improved control of amyloid beta (Aβ) plaques, alterations in microglial activation status, decreased levels of neuritic dystrophy, and protection against cognitive decline. Moreover, rescue of neurological disease in STING-deficient 5xFAD mice was characterized by reduced expression of type I interferon signaling genes in both microglia and excitatory neurons.

DISCUSSION: These findings reveal critical roles for STING in Aβ-driven neurological disease and suggest that STING-targeting therapeutics may offer promising strategies to treat AD.

KEYWORDS
Alzheimer's disease, amyloid beta, amyloidosis, innate immunity, microglia, neurodegenerative disease, neuroimmunology, STING

Highlights

- Stimulator of interferon genes (STING) deficiency in the 5xFAD mouse model of Alzheimer's disease-related amyloidosis results in decreased amyloid beta (Aβ) deposition and altered microglial activation status.
- Protection against amyloidosis in STING-deficient 5xFAD mice is associated with decreased expression of genes involved in type I IFN signaling, improved neuronal health, and reduced levels of oxidative stress.
- Loss of STING in 5xFAD mice leads to improved spatial learning and memory.

1 | BACKGROUND

Alzheimer's disease (AD) is a debilitating neurodegenerative disease that is characterized by pathological deposition of amyloid beta (Aβ) aggregates and tau tangles, neuronal loss, and cognitive decline. In recent years, there has been growing appreciation for the role that the innate immune system plays in AD pathogenesis.[1–5] Most notably, human genetics studies have revealed that many of the top genetic risk factors linked to late-onset AD are immune genes and/or are expressed predominantly by microglia in the brain,[6–8] which are the primary immune cell population that surveys the brain for pathogens and other harmful agents. Emerging from recent work is the generalized idea that some level of controlled innate immune activation is needed, especially early in AD progression, to mobilize microglial responses to aid in the containment and disposal of neurotoxic Aβ aggregates.[1–5] However, the innate immune response in AD also needs to be held in check as chronic and/or dysregulation of innate immune signaling pathways can lead to aberrant neuroinflammation, microglial dysfunction, and neurodegenerative disease progression.[1–5]

While innate immune signaling has been increasingly linked to AD pathogenesis, the roles of many discrete innate immune signaling pathways in driving AD progression have not been investigated using genetic targeting approaches to date. One such molecule is stimulator of interferon genes (STING), which is a major innate immune adaptor molecule that is best known for orchestrating immune signaling in response to both pathogen- and host-derived DNA that finds its way into the cytosol following infection, mitochondrial compromise, and genomic stress.[9–11] STING activation in response to genotoxic stress or pathogen-derived cytosolic DNA requires cyclic GMP–AMP synthase (cGAS), a cytosolic DNA sensor that generates the STING-activating second messenger cyclic GMP–AMP (cGAMP).[12–15] Once activated, STING potently induces the production of type I interferons (IFNs) and nuclear factor kappa-light-chain-enhancer of activated B cells (NF-κB)-mediated cytokines such as interleukin-6 (IL-6) and tumor necrosis factor-α (TNF-α). Engagement of cGAS-STING signaling following detection of cytosolic DNA has been shown to be critically involved in the generation of protective immune responses against multiple pathogens and forms of cancer.[9–11] However, aberrant activation of cGAS-STING in response to genotoxic stress has also been shown to be a key contributor to detrimental inflammation and tissue damage in aging, as well as various autoinflammatory and autoimmune disorders.[9–11]

Recent studies have also begun to define instrumental roles for cGAS and STING in multiple neurodegenerative diseases, including amyotrophic lateral sclerosis,[16] primary tauopathies,[17] Parkinson's disease,[18] and aging-associated dementia.[19] Here, it has largely been shown that knocking down cGAS and/or STING leads to an attenuation of neuroinflammatory responses and protection against neuronal cell loss.[20] There have also been recent attempts to explore how STING impacts amyloidosis using the pharmacological agent H-151.[21,22] However, additional studies involving genetic deletion of STING are still needed as H-151 has been reported to have off-target effects and can inhibit multiple innate immune pathways in addition to abrogating STING.[23,24]

To this end, in the present study, we explored how genetic ablation of STING impacts Aβ amyloidosis progression in the 5xFAD mouse model of AD. Here, we found that deletion of STING in 5xFAD mice leads to improved control of Aβ load, alterations in microglial activation status, and protection against neuritic dystrophy and cognitive decline. Moreover, the rescue of amyloidosis-related disease parameters in STING-deficient mice was accompanied by a shift from AD-associated transcriptional programming toward a more homeostatic profile in STING-deficient cell populations, as evidenced by the decreased expression of antiviral and type I IFN response genes, as well as the increased expression of genes associated with synaptic signaling and cognitive resilience in microglia and excitatory neurons. Overall, our results suggest that STING drives Aβ accumulation, microglial activation, and neuronal dystrophy in Aβ-associated neurological disease, highlighting its potential as a therapeutic target in the treatment of AD.

2 | METHODS

2.1 | Mice

All mouse experiments were performed in accordance with the relevant guidelines and regulations of the University of Virginia and approved by the University of Virginia Animal Care and Use Committee. 5xFAD (Strain #034848-JAX)[25] and *Sting1*$^{-/-}$ mice (Strain #025805-JAX)[26] were obtained from the Jackson Laboratory and crossed to generate *Sting1*$^{+/+}$ (denoted as WT), *Sting1*$^{-/-}$ (denoted as St^{KO}), 5xFAD *Sting1*$^{+/+}$ (denoted as 5xFAD), and 5xFAD *Sting1*$^{-/-}$ (denoted as 5xSt^{KO}) female mice to be used in subsequent experiments. Mice were housed with food and water available ad libitum, under specific pathogen-free conditions with controlled temperature (21 ± 1.5°C) and humidity (50 ± 10%), and subjected to the standard 12-h light/dark cycle.

2.2 | Morris water maze behavior testing

All mice were 4 months old at the time of behavior testing. All behavior experiments were performed between 12 and 6 p.m. in a blinded fashion. Mice were transported from their home vivarium room to the behavior core and habituated for at least 30 min in the respective testing rooms before each test. Mice were then transported back to their home vivarium room once testing was completed. All tests were tracked and scored using Ethovision XT video tracking software (Noldus). Spatial learning and memory were evaluated using the Morris water maze (MWM) test as previously described.[27] Briefly, mice underwent training for 4 days with four trials per day, and then mice were tested once on Day 5 as part of the probe phase. Mice were trained in an opaque pool of diluted white paint, with four distinct visual cues along the walls and a hidden platform placed 1 cm below the water surface. Starting points for each trial were alternated relative to visual cues. Trials ended when mice successfully located the hidden platform or after 60 s of testing. Mice that failed were retrained by being placed on top of the platform for 5 s after a given trial. The latency to escape, the number of times on the platform, and the time spent on the platform were among the many measures of this test.

2.3 | Brain sample preparation

Mice were euthanized by CO_2 asphyxiation followed by cervical dislocation and then mice were transcardially perfused with 20 mL of 1× Dulbecco's phosphate-buffered saline without calcium and magnesium (1× DPBS; Gibco #14190144). Brains were dissected out and bisected, with the right hemisphere snap-frozen and stored for long-term use at −80°C, while the left hemisphere was drop-fixed in 4% paraformaldehyde (PFA; Electron Microscopy Sciences #15714-S) in 1× Dulbecco's phosphate buffered saline (DPBS) overnight at 4°C. Fixed brains were rinsed in 1× DPBS and dehydrated in 30% sucrose in 1× DPBS for 48 h at 4°C. Dehydrated brains were mounted in Tissue-Tek OCT compound (Sakura #4583) and sectioned at 50 µm sagittally using a cryostat (Leica #CM1950). Sections were stored in 0.05% sodium azide (Ricca Chemical #71448-16) in 1× DPBS at 4°C for immunofluorescence (IF) microscopy experiments. Flash-frozen brains were thawed and mechanically homogenized in 500 µL Tissue Protein Extraction Reagent (T-PER; Thermo Fisher #78510) supplemented with PhosSTOP phosphatase inhibitor cocktail (Roche #C764L25) and cOmplete protease inhibitor cocktail (Roche #11-697-498-001).

RESEARCH IN CONTEXT

1. **Systematic review**: The authors reviewed previous peer-reviewed publications using traditional sources (e.g., PubMed). While there have been recent studies exploring the effects of the pharmacological agent H-151 in the 5xFAD mouse model of Alzheimer's disease (AD)-associated amyloidosis, rigorous studies involving genetic deletion of STING are still needed in the field. Most notably, like most pharmacological inhibitors, H-151 has been reported to inhibit multiple diverse molecular pathways in addition to abrogating stimulator of interferon genes (STING).
2. **Interpretation**: Our results demonstrate that genetic ablation of STING in 5xFAD mice leads to improved control of amyloid beta (Aβ) pathology, altered microglial activation, and protection against cognitive decline and neuronal dystrophy. Unbiased single-nuclei RNA-sequencing (snRNA-seq) studies further revealed that neurological disease protection in STING-deficient 5xFAD mice is characterized by increased expression of neuronal health genes in excitatory neurons as well as decreased expression of antiviral and type I interferon (IFN) response genes in both neurons and microglia.
3. **Future directions**: Our studies provide a foundation for further investigation into how STING signaling contributes to Aβ amyloidosis. Additional studies are needed to interrogate in which specific cell types STING functions to impact Aβ-mediated neurodegenerative disease progression. Future research endeavors are also needed to uncover the key upstream DNA damage sensors and molecular events that activate STING during AD. While DNA damage sensing by cyclic GMP–AMP synthase (cGAS) is the most extensively studied upstream activator of STING, other genomic sensors and cellular danger signals have also been reported to trigger STING activation independently of cGAS. For instance, emerging evidence indicates that defects in vesicle trafficking and endolysosomal dysfunction can trigger STING-dependent neurodegenerative disease independently of genomic sensing by cGAS.

2.4 | Immunofluorescence

Floating brain sections were transferred from 0.05% NaN_3 in 1× PBS and blocked and permeabilized in 2% donkey serum, 1% bovine serum albumin (BSA), 0.1% Triton-X, and 0.05% Tween-20 in 1× PBS (IF buffer) for 2 h at room temperature while rocking. Sections were then incubated in primary antibodies in IF buffer overnight at 4°C, while rocking. Stained sections were washed in 0.05% Tween-20 in 1× PBS (wash buffer) 3 times, for 10 min each and at room temperature (RT), while rocking. Sections were subsequently incubated in secondary antibodies in IF buffer for 2 h at RT while rocking. All secondary antibodies were raised in donkey and conjugated to Alexa Fluor fluorophores (1:1,000; e.g., Invitrogen #A-31571). Sections were washed 3 times for 10 min each at RT with rocking and then sections were counterstained with Thioflavine S (ThioS) or DAPI. For ThioS staining, sections were incubated in 0.2 mg/mL ThioS in 50% EtOH while rocking for 8 min at RT, washed three times in only 50% EtOH for 2 min each, transferred to deionized (DI) water, and then to 1× DPBS. For DAPI staining, sections were incubated in 20 µg/mL DAPI in 1× DPBS while rocking for 10 min at RT and transferred to 1× DPBS. Counterstained sections were then mounted using ProLong Gold antifade reagent (Invitrogen #P36930) onto charged glass microscope slides (Fisherbrand #12-550-15) and under cover glass (Fisherbrand #12-544C). Mounted slides were cured for at least 24 h and stored at 4°C until imaging on the SP8 confocal microscope (Leica Microsystems) and the Leica Application Suite (LAS) X microscope software (Leica Microsystems, v3.5.5.19976).

All confocal images were acquired in eight-bit format, at 1024 × 1024 pixel resolution, and with 1.0× digital zoom unless specified otherwise. For cortical measures, three to four fields of view were selected within layers with the densest plaque burden. Aβ total coverage images were acquired by tile scanning entire brain sections at 10× magnification, with 1.0× digital zoom and 0.5 µm *z*-slices. Images of cortical Aβ plaque and fibril burden, microgliosis, dystrophic neurites (DNs) were acquired at 63× magnification, with 0.75× digital zoom and system-optimized *z*-slices. AXL occupancy images were acquired at 40× magnification with 0.75× digital zoom and system-optimized *z*-slices. Terminal deoxynucleotidyl transferase dUTP end labeling (TUNEL) images were acquired at 40× magnification with 1.0× digital zoom and system-optimized *z*-slices.

2.5 | Image analysis

All image analyses were performed using FIJI or Imaris software (v9.5.1; unless specified otherwise; Oxford Instruments). Total Aβ coverage was assessed by creating max projections, drawing regions of interest (ROIs) in the DAPI channel, automatically thresholding images, and measuring percent area of D54D2 in FIJI. Plaque burden was assessed by measuring count, intensity, volume, overlap, and proximity using the "surfaces" function in Imaris.

Total microglial coverage was assessed according to total Aβ coverage analysis methods above, by using the same ROI and measuring percent area of IBA1 in FIJI. Microglial count and volume were quantified using the "spots" and "surfaces" features in Imaris software, respectively. Microglial recruitment to plaques was assessed by filtering detected spots within 15 and 30 µm of Aβ plaque surfaces. Microglial activation state was assessed using the "surfaces" feature in Imaris software by rendering IBA1+ and CD68+ volumes and calculating the percentage volume of IBA1+ CD68+ per total IBA1+ volume. Sholl analysis was performed on cells farther than 30 µm away from plaque surfaces for consistency and accuracy of the segmentation. ROIs were created for 15 cells per animal from across three sections and six to nine images. Branches were detected using a machine learning algorithm in Imaris (v10.0.0) and verified manually using the IBA1 channel. AXL occupancy was assessed in FIJI by manually counting IBA1+ cells and IBA1+ AXL+ double-positive cells and calculating the percentage of IBA1+ AXL+ cells per total IBA1+ cells. STAT1 occupancy was assessed in FIJI in the same manner.

Amyloid precursor protein positive (APP+) DNs and ThioS+ plaques were rendered using the "spots" and "surfaces" features in Imaris software, respectively. DNs within 15 and 30 µm of plaques were identified and counted to determine DNs per plaque. Cell death was assessed in the CA1 hippocampal region by determining the area of TUNEL+ puncta within neuronal nuclei (NeuN) regions in FIJI.

2.6 | Protein extraction

Homogenates were centrifuged at 16,000 rpm for 10 min at 4°C to yield a supernatant and pellet containing soluble and insoluble proteins, respectively. To isolate proteins from pellets, 25 µL of pellets were incubated in 5 M guanidine-hydrochloride solution (Gu-HCl; Thermo Fisher #24115) in 50 mM Tris base (pH = 8.0) for 3 h at room temperature, with vigorous agitation on a laboratory rocker. Mixtures were diluted 1:8 in 1X PBS with PhosSTOP and cOmplete and centrifuged at 16,000 g for 20 min at 4°C, and supernatants were collected to recover insoluble proteins. Total soluble and insoluble protein were quantified using the Protein660 reagent (Thermo Fisher #22660) according to manufacturer instructions and stored at −80°C for later use.

2.7 | Aβ levels

Soluble and insoluble protein lysates were diluted in 1X PBS at 1:10 and 1:1,000, respectively. Aβ42 levels were measured by sandwich enzyme-linked immunosorbent assay (ELISA; Invitrogen #KMB3441) according to manufacturer instructions. Briefly, samples and standards were added to strips and incubated with detector antibody solution. Strips were washed, and IgG HRP solution was added to strips. Wash steps were repeated, and stabilized chromogen solution was added to strips. Stop solution was added and plates were read at 450 nm using a plate reader. Aβ42 concentrations were determined using a standard curve and normalized to total protein levels.

2.8 | Lipid peroxidation

Lipid peroxidation was measured using the malondialdehyde (MDA; Abcam #118970) assay according to manufacturer instructions. Whole-brain soluble protein lysates were diluted 1:10 in 1× PBS prior to the assay. Briefly, samples and standards were incubated with thiobarbituric acid (TBA) for 60 min at 95°C and cooled in an ice bath for 10 min. MDA concentrations were determined using a standard curve and normalized to total protein levels.

2.9 | snRNA-seq and analysis

Brains were collected from mice via rapid decapitation to minimize transcriptional changes. Cortical samples were microdissected, flash-frozen, and stored at –80°C. Pooled cortical samples were submitted to GENEWIZ (Azenta Life Sciences) for processing and RNA sequencing. Nuclei were isolated to generate single-nuclei 3′ RNA libraries using the Chromium Single Cell 3′ Reagent Kit (10X Genomics). Libraries were sequenced on the HiSeq 4000 (Illumina), and raw FASTQ files were processed with the Cell Ranger (v7.0.1, 10X Genomics) pipeline using the mm10 mouse reference genome.

The Cell Ranger output folders were used to construct AnnData objects which were analyzed in Python (v3.9.18) using the Scanpy (v1.9.8) framework.[28] Low-quality nuclei were excluded if they: (a) expressed $<$ 1k or $>$ 95th percentile for total transcript count, (b) expressed $<$ 500 or $>$ 97th percentile for uniquely expressed genes, (c) contained $>$ 5% mitochondrial reads, or (d) had $>$ 99th percentile for ribosomal genes. Doublets were scored with Scrublet (v0.2.3)[29] and further confirmed with SOLO,[30] and doublet nuclei were removed. Scanpy's library size normalization was performed on the concatenated dataset,[28] followed by log-transformation and scaling after selecting for and annotating the top 3k highly variable genes. scVI-tools (v1.1.2)[31] was used to integrate the samples using the raw counts layer and construct a latent representation used for clustering. Nuclei were grouped into clusters using the Leiden algorithm using default settings, and UMAP was applied for dimensionality reduction and visualization. Marker genes were identified using Scanpy's implementation of the Wilcoxon rank-sum test,[28] and clusters were annotated based on the resulting scores of well-established cell type-specific markers (e.g., *Rbfox3*, *Slc17a6*, *Gad1*, *Sox10*). Differential expression (DE) analysis was performed using diffxpy (v0.7.4) for annotated cell types and Leiden clusters with sufficient nuclei ($>$ 40 per group) and balanced group sizes, wherein groups with fewer than 10% of the total cells tested were excluded. Wald testing was used to identify differentially expressed genes (DEGs), and the results output was filtered to exclude genes with log2 fold change magnitudes $>$ 100 and zero or negligible gene expression between testing groups, indicative of transcript sampling artifacts.

All data visualizations were performed in R. UMAP visualizations and feature plots, as well as heat maps, were generated using the Seurat package to visualize clusters, marker gene expression, and the top conserved genes expressed by each cell type. To minimize ambient RNA artifacts, genes canonically restricted to neurons (e.g., *Snap25*, *Slc17a7*) were excluded from microglial DEGs based on prior reports of common snRNA-seq contamination.[32,33] Volcano plots were generated using the EnhancedVolcano package to visualize key DE results. Pathway analyses were performed in g:Profiler using DEGs with adjusted *p*-values of less than 0.05 and $\log_2$ fold changes of ± 0.5. Relevant pathways within the top 10 highlighted by g:Profiler were selected and plotted in Prism.

2.10 | Statistical analyses

Mean values, standard error mean (SEM) values, Student's *t* test (unpaired), and one-way analysis of variance (ANOVA) were calculated using Prism software (GraphPad). Nested data were analyzed by linear mixed-effects models using the "lme4" package in R (R Core Team). *p*-values less than 0.05 were considered significant.

3 | RESULTS

3.1 | Loss of STING leads to improved control of Aβ load

Studies conducted on human postmortem samples have shown that AD brains routinely display increased levels of DNA damage and hyperactive STING signaling when compared to age-matched controls.[17,21,34–36] However, in vivo studies have not yet been conducted to interrogate how genetic ablation of STING affects AD-related pathogenesis. Therefore, to explore a role for STING in Aβ-mediated disease in vivo, we crossed germline STING-deficient mice with 5xFAD mice, the latter of which is a widely used model of AD-associated amyloidosis. We first evaluated the impact of STING deletion on total Aβ burden in 5xFAD mice by performing IF staining using the D54D2 antibody on sagittal brain sections isolated from 5-month-old 5xFAD *Sting1*$^{-/-}$ mice (abbreviated as 5xSt^{KO}) and their 5xFAD *Sting1*$^{+/+}$ littermate controls (abbreviated as 5xFAD). In these studies, we observed decreased percent area covered by Aβ staining in the cortex, hippocampus, and subiculum regions of 5xSt^{KO} mice when compared to 5xFAD controls (Figure 1A–D). Consistent with the improved control of total Aβ load seen with STING deficiency in 5xFAD mice, we also observed reductions in total Aβ plaque counts in the cortices of 5xSt^{KO} mice by Thioflavine S (ThioS) staining relative to 5xFAD littermate controls at both 5 (Figure 1E,F) and 9 months of age (Figure S1A,B). To further confirm these results by a molecular approach, we next measured the levels of Aβ1-42, which is a neurotoxic Aβ species shown to drive neuronal dysfunction and death in AD, in half-brain lysates by ELISA. Here, we detected lower levels of both soluble (T-PER fraction; Figure 1G) and insoluble (Gu-HCL fraction; Figure 1H) Aβ1-42

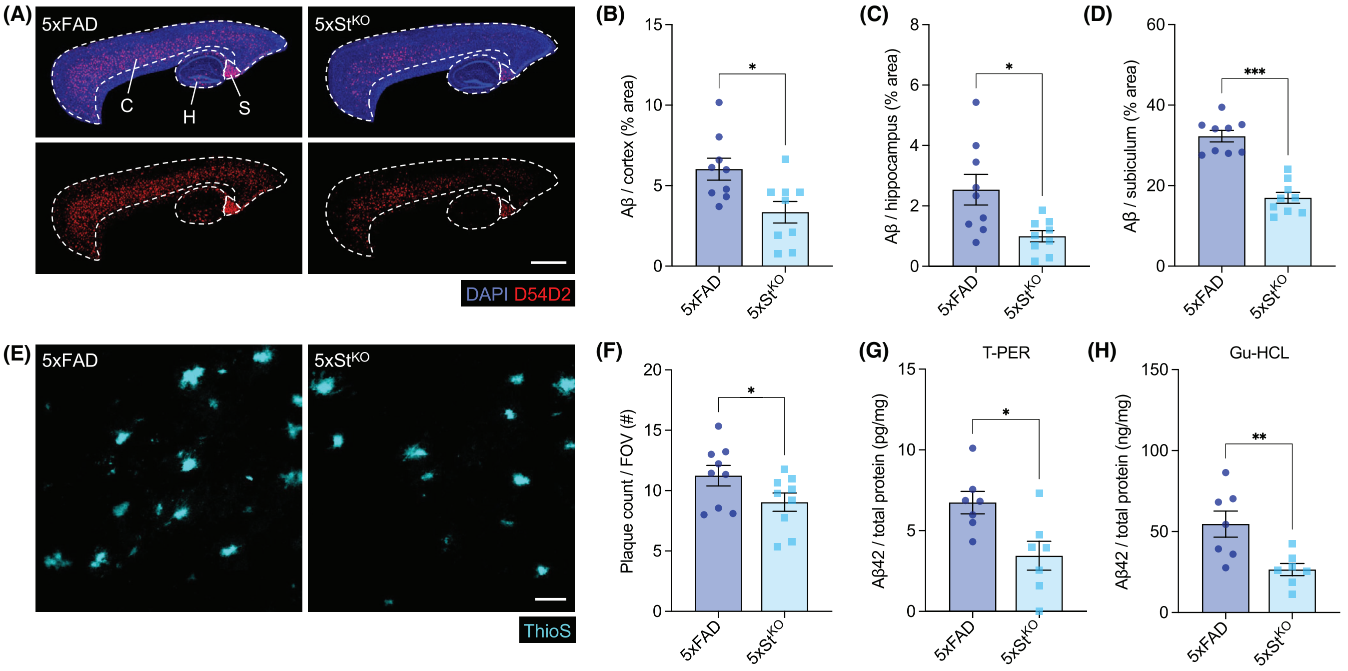

FIGURE 1 Amyloid beta load is reduced with STING deletion in 5xFAD mice. 5xFAD *Sting1*$^{-/-}$ (abbreviated as 5xSt^{KO}) mice and littermate 5xFAD *Sting1*$^{+/+}$ (abbreviated as 5xFAD) controls were harvested at 5 months of age to evaluate Aβ load by IF imaging. (A–D) Analysis of total Aβ burden in the cortex, hippocampus, and subiculum ($n = 9$ mice/group, six to nine images/mouse, two independent experiments). (A) Representative confocal images of brain sections stained for nuclei (DAPI, blue) and total Aβ (D54D2, red; scale bar = 40 μm) in the cortex (abbreviated as 'C'), subiculum (abbreviated as 'S'), and hippocampus (abbreviated as 'H'). Quantification of percent area covered by D54D2 staining in the cortex (B), hippocampus (C), and subiculum (D). (E,F) Analysis of cortical Aβ plaque burden ($n = 9$, 9–12 images/mouse, three independent experiments). (E) Representative confocal images of brain sections stained for Aβ plaques (ThioS, cyan; scale bar = 30 μm). (F) Quantification of plaques per FOV. (G,H) Analysis of Aβ42 protein concentrations from whole-brain lysates ($n = 13$–15 mice/group, three independent experiments). (G) ELISA quantification of Aβ42 per total protein from the soluble fraction extracted with T-PER and (H) the insoluble fraction extracted with Gu-HCL. Statistical significance between experimental groups was calculated by linear mixed-effects models (B–D,F) and unpaired Student's *t* test (G,H). Data points represent individual mice and error bars represent mean ± SEM. $^{*}p < 0.05$, $^{**}p < 0.01$, $^{***}p < 0.001$. Aβ, amyloid beta; DAPI, 4',6-diamidino-2-phenylindole; ELISA, enzyme-linked immunosorbent assay; FOV, field of view; IF, immunofluorescence; SEM, standard error of the mean; STING, stimulator of interferon genes.

in the brains of 5-month-old 5xSt^{KO} mice when compared to 5xFAD littermate controls. In total, these data suggest that genetic ablation of STING leads to improved control of Aβ load in 5xFAD mice.

3.2 | Microgliosis is blunted with STING deletion in Aβ amyloidosis

Dysregulated microglial responses have been shown to contribute to AD pathogenesis and a host of other brain disorders.[1–5] In AD, microglia are recruited toward plaque-rich regions where they proliferate and adopt an activated state. To assess whether STING influences microgliosis in AD, we performed IF staining to evaluate IBA1+ macrophage/microglia coverage, activation state, and morphology in regions enriched with Aβ plaques. In these studies, we found that the absence of STING in 5-month-old 5xFAD mice leads to decreased area covered by IBA1+ macrophages in the cortex, hippocampus, and subiculum when compared to age-matched 5xFAD controls (Figure 2A–D). Consistent with the decrease in percent area coverage of IBA1+ staining seen throughout the brains of 5xSt^{KO} mice, we also detected fewer numbers of IBA1+ macrophages in the cortices of STING-deficient 5xFAD mice relative to littermate 5xFAD controls at both 5 months of age (Figure 2E,F) and 9 months of age (Figure S2A–C). Moreover, we also observed lower numbers of IBA1+ cells within 15 and 30 μm of Aβ plaques in 5xSt^{KO} mice relative to 5xFAD controls, both at 5 months of age (Figure 2E,G) and into advanced stages of amyloidosis (9 months of age; Figure S2D–E). Taken together, these findings indicate that genetic ablation of STING in the 5xFAD mouse model of amyloidosis leads to reduced total numbers of IBA1+ macrophages throughout the brain. Importantly, these differences in microgliosis appear to be specifically in response to amyloidosis, and not the result of a baseline effect of STING deletion on microglial biology, as IBA1+ macrophage numbers, volume, and staining intensity were all found to be similar between STING-deficient (abbreviated as St^{KO}) and wild-type (WT) mice that lack the 5xFAD transgenes and do not develop amyloidosis (Figure S3A–D).

Given the effects seen with STING deletion on microglial numbers in amyloidosis, we were next interested in determining whether the absence of STING also impacted microglial activation status in 5xFAD mice. To this end, we first evaluated the expression levels of

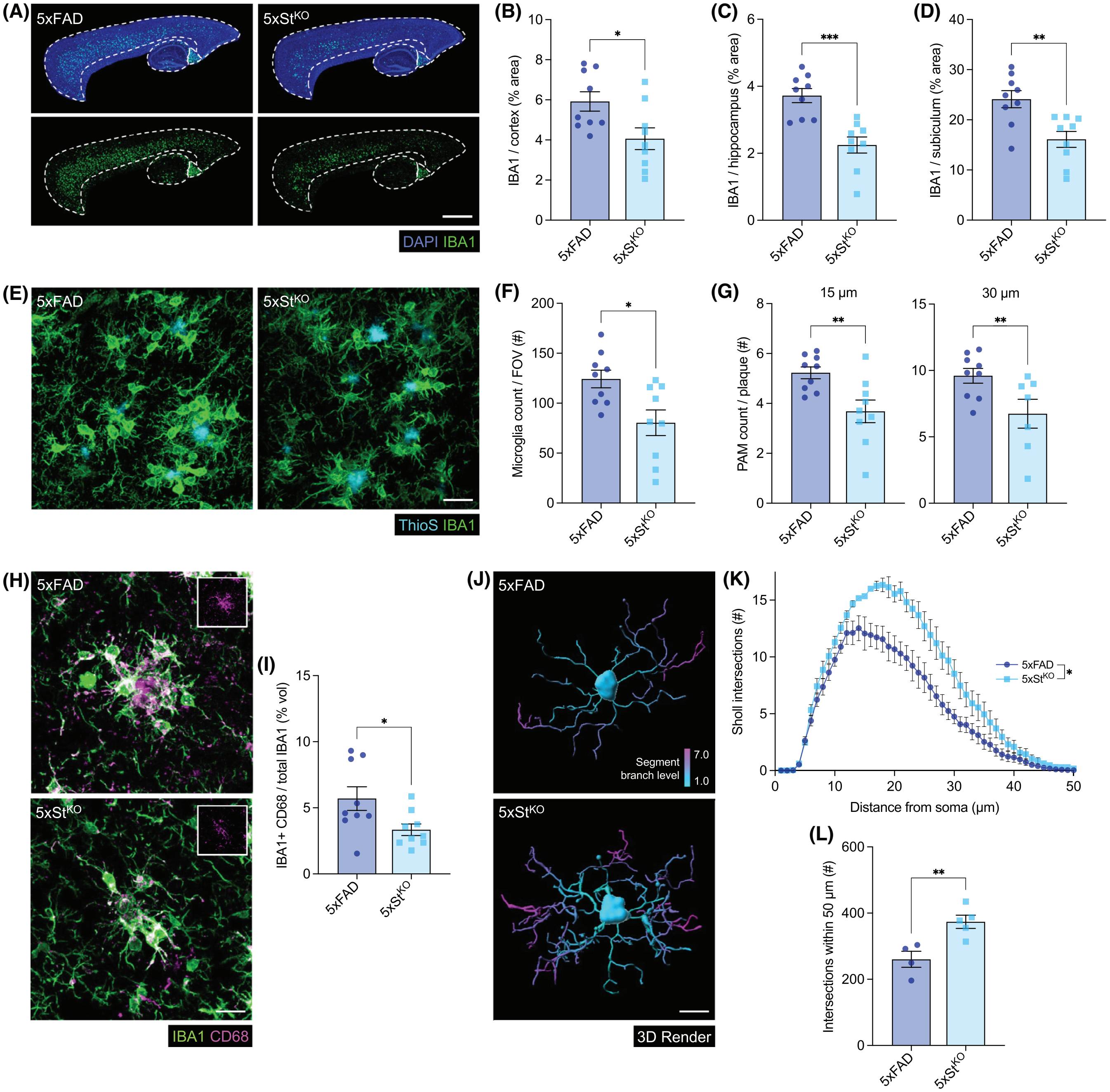

FIGURE 2 Genetic ablation of STING dampens microgliosis in 5xFAD mice. (A–L) 5xSt^{KO} mice and 5xFAD littermate controls were harvested at 5 months of age to evaluate microglial numbers and CD68 phagolysosomal marker expression by immunofluorescence staining. (A–G) Analysis of microglial coverage and recruitment to Aβ plaques ($n = 9$ mice/group, 9–12 images/mouse, three independent experiments). (A) Representative confocal images of brain sections stained for nuclei (DAPI, blue), plaques (ThioS, cyan), and macrophages/microglia (IBA1, green; scale bar = 30 µm). Quantification of percent area covered by IBA1+ staining in the (B) cortex, (C) hippocampus, and (D) subiculum. (E) Representative confocal images of PAMs (IBA1, green) and plaques (ThioS, cyan; scale bar = 15 µm). (F) Enumeration of IBA1+ cells per FOV in the cortex. (G) Number of PAMs within 15 and 30 µm of plaque surfaces. (H,I) Analysis of CD68 phagolysosomal marker expression ($n = 8$–9 mice/group, 9–12 images/mouse, three independent experiments). (H) Representative confocal images of brain sections stained for microglia (IBA1, green) and the phagolysosomal marker CD68 (magenta; inset FOV; scale bar = 15 µm). White regions denote colocalization of CD68 and IBA1 staining. (I) Quantification of CD68 staining colocalized with IBA1 staining. (J–L) Sholl analysis of cortical microglia ($n = 4$–5 mice/genotype, 15 cells/mouse from six to nine images each, three independent experiments). (J) Representative 3D rendering of IBA1+ cells (iscale bar = 10 µm). (K) Quantification of total Sholl intersections at various distances away from the cell soma and (L) total number of intersections within 50 µm of the cell soma. Statistical significance between experimental groups was calculated by linear mixed-effects models. Data points in the column graphs (B–D, F, G, I, and L) represent individual mice, and data points in the line graph (K) represent means for each experimental group. Error bars represent mean ± SEM. $^{*}p < 0.05$, $^{**}p < 0.01$, $^{***}p < 0.001$. Aβ, amyloid beta; DAPI, 4′,6-diamidino-2-phenylindole; FOV, field of view; PAMs, plaque-associated microglia; SEM, standard error of the mean; STING, stimulator of interferon genes.

the phagolysosomal marker CD68 as it has been extensively associated with microglial activation in multiple neurological disease models. Here, we found that CD68 expression by cortical IBA1+ macrophages is attenuated in 5xSt^{KO} mice when compared to 5xFAD controls at both 5 (Figure 2H–I) and 9 months of age (Figure S2D,F). Importantly, these differences in CD68 expression appear to be in response to amyloidosis, as the levels of CD68 expression were largely indistinguishable between WT and St^{KO} mice that are not on the 5xFAD background (Figure S3E–H). To further interrogate the impact of STING ablation on microglial activation, we next performed Sholl analysis to evaluate microglial morphology, which is often used as a surrogate marker of activation state. Here, we found that IBA1+ macrophages in 5xSt^{KO} mice display more complex branching patterns (i.e., greater numbers of Sholl intersections) compared to their 5xFAD counterparts, indicating that they maintain a ramified morphology classically associated with more homeostatic conditions (Figure 2J–L). Taken together, these imaging results suggest that the absence of STING impacts microglial numbers, recruitment toward plaques, and activation status in response to Aβ accumulation.

3.3 | STING deletion in amyloidosis leads to dampened expression of innate immune genes by microglia

To gain more comprehensive and unbiased insights into how STING influences AD-associated amyloidosis, we next performed single-nuclei RNA sequencing (snRNA-seq) on cortical brain samples from 6-month-old 5xSt^{KO} mice and 5xFAD littermate controls. Nuclei across both genotypes were arranged by uniform manifold approximation and projection (UMAP) for visualization, and nine clusters were manually defined based on the expression of cell type-specific signature genes as astrocytes, endothelial cells, excitatory (Ex.) neurons, inhibitory (In.) neurons, microglia (MG), oligodendrocytes (Oligo.), oligodendrocyte progenitor cells (OPC), other neurons (Neur.), and an unidentified (Unknown) cell population characterized by high expression of *Cped1*, *Eya2*, and *Foxd1* (Figure 3A,B and Figure S4). Similar numbers of nuclei were recovered from both genotypes and the relative distribution of nuclei across most clusters was similar between 5xSt^{KO} and 5xFAD mice (Figure 3C). However, we did note the presence of higher proportions of excitatory neurons in 5xSt^{KO} mice, whereas 5xFAD littermate controls exhibited higher relative frequencies of inhibitory neurons (Figure 3C).

In light of our IF imaging data demonstrating altered numbers and activation status of microglia in 5xFAD mice that lack STING (Figure 2), we were intrigued to explore how STING shapes microglial gene expression. Focusing on this population, we identified 34 DEGs between 5xSt^{KO} and 5xFAD microglia (Figure 3D). Notably, we observed that STING-deficient microglia exhibit reduced expression of multiple innate immune (*Axl*, *Cd83*, and *Ptgds*) and type I IFN response genes (*Ifi204*, *Irak2*, *Stat1*, *and Trim30a/d*), alongside increased expression of genes associated with synaptic function and microglial homeostasis (*Slc1a2* and *Fcrls*, respectively) (Figure 3D). In line with this, gene ontology (GO) pathway analysis based on differentially expressed genes (DEGs) also revealed an enrichment of innate immune and antiviral response pathways in 5xFAD microglia (Figure 3E). To validate our transcriptomic results and assess differential expression at the protein level, we next performed IF staining for AXL (Figure 3F–I) and STAT1 (Figure 3J–M), both of which were transcriptionally downregulated in 5xSt^{KO} microglia in our snRNA-seq dataset (Figure 3D). In these separate studies, we found fewer AXL+ or STAT1+ microglia in total, as a percentage of total microglia, and in proportion to the number of plaques (Figure 3F–M). Taken together, these findings indicate that genetic ablation of STING in 5xFAD mice leads to a distinct microglial transcriptional profile characterized by dampened innate immune and type I IFN signaling, along with enhanced synaptic support and a restoration of homeostatic gene expression.

3.4 | Loss of STING in 5xFAD mice promotes improved neuronal health and limits cognitive decline

We were next interested in exploring how STING deletion affects neuronal health, as neuronal damage is a critical step in AD progression and precedes neuronal loss and cognitive decline. We turned our attention to excitatory neuron gene expression, as excitatory neuron dysfunction has been identified as a pivotal contributor to cognitive decline in AD. To this end, we leveraged our snRNA-seq dataset to assess the extent to which STING deletion shapes gene expression in the excitatory neuron cluster (Figure 4A). Here, we found that 5xSt^{KO} excitatory neurons exhibit increased expression of genes associated with synaptic signaling and calcium regulation (e.g., *Camk2a*, *Mef2c*, *Slc17a7*, and *Slc1a2*), neuronal maturation and protection (e.g., *Nrgn*, *Rbfox3*, *Cck*, and *Snca*), and cell adhesion (e.g., *Col5a1* and *Atp8b1*) (Figure 4B,C). The increase in *Mef2c* expression exhibited by STING-deficient excitatory neurons is particularly notable as *MEF2C* is an AD risk gene that is necessary for neuronal survival.[37,38] We also observed reduced expression of genes related to Aβ binding and toxicity (e.g., *Erbb4*), phosphodiesterase activity (e.g., *Pde1c* and *Pde3a*), inflammatory signaling (e.g., *Il16*, *Ror2*, and *Aim2*), and IFN-related pathways (e.g., *Ifitm10* and *Irf3*) in STING-deficient excitatory neurons (Figure 4B,C). Of note, *Erbb4* has been shown to drive Aβ accumulation, neurotoxicity, and cognitive decline in AD mouse models,[39–42] making its downregulation particularly compelling. Taken together, these data suggest that global STING deletion in 5xFAD mice promotes the expression of genes supporting neuronal function while blunting type I IFN-associated pathways in excitatory neurons.

Based on our snRNA-seq data identifying increased expression of genes and pathways associated with neuronal health in 5xFAD mice that lack STING (Figure 4B,C), we were next interested in validating whether this corresponded with physical signs of neuronal resilience. As a first approach to interrogate this, we evaluated the formation of DNs by quantifying the levels of APP puncta surrounding Aβ plaques in the cortices of 5xSt^{KO} mice and 5xFAD littermate controls. DNs are swollen neuronal processes that form around Aβ plaques and accumulate organelles and proteins, namely APP, and lead to impaired axonal

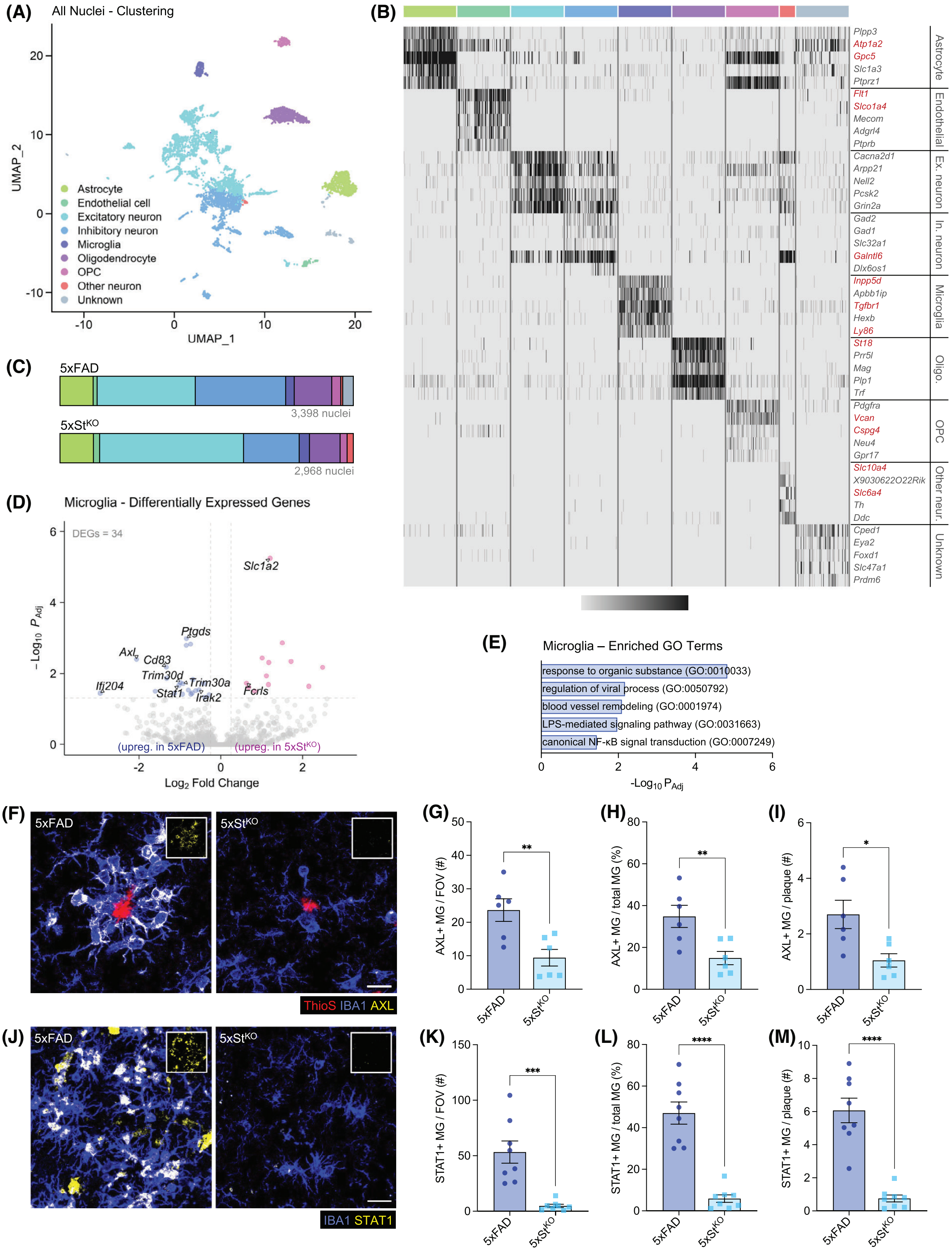

FIGURE 3 Lack of STING in 5xFAD mice leads to altered microglial activation status. (A–E) Gene expression was assessed in 6-month-old 5xFAD and 5xSt^{KO} mice by pooled snRNA-seq of cortical tissue ($n = 3$ per pooled sample). (A) UMAP plot of cells grouped by major brain cell type. Clusters were manually defined based on the expression of cell type-specific signature genes. (B) Heat map depicting an unbiased list of the 5 most highly expressed genes in each cell cluster. The genes highlighted in red are those that have been previously linked to AD in humans. (C) Quantification of numbers of nuclei sequenced per genotype and visual breakdown by cell type. (D) Volcano plot depicting DEGs (upregulated, pink; downregulated, blue) in the microglia cluster of 5xSt^{KO} versus 5xFAD cortex. Colored points depict genes with adjusted *p*-values less than

transport and neuronal damage. Consistent with our snRNA-seq findings demonstrating elevated expression of neuronal health genes in aged $5xSt^{KO}$ mice, we also observed signs of attenuated neuritic damage with STING deletion in 5-month-old 5xFAD mice as indicated by the reduced numbers of DNs detected within 15 and 30 µm of Aβ plaques relative to 5xFAD controls (Figure 4D,E). Moreover, we also found that the protection against neuritic dystrophy seen in STING-deficient 5xFAD mice extended out to the later stages of amyloidosis. More specifically, we continued to observe reduced levels of APP+ DNs out to 9 months of age in $5xSt^{KO}$ mice when compared to 5xFAD littermate controls (Figure S5A–B).

Lipid peroxidation and oxidative stress have also been increasingly linked to neuronal dysfunction and cell death in AD and other neurodegenerative diseases.[43–45] Therefore, to evaluate whether STING deletion alters lipid peroxidation status in the brains of 5xFAD mice, we measured levels of MDA, which is a reactive byproduct of lipid peroxidation and a marker of oxidative stress reported to be elevated in AD brains.[46] In these studies, we detected lower levels of MDA in whole-brain lysates from 5-month-old STING-deficient 5xFAD mice in comparison to 5xFAD littermate controls (Figure 4F), suggesting that reduced levels of lipid peroxidation are also a hallmark of the improvements in neuronal health seen in $5xSt^{KO}$ mice. Likewise, we also observed that this protection against lipid peroxidation and oxidative stress remained in STING-deficient 5xFAD mice out to 9 months of age (Figure S5C).

Decline in neuronal health can eventually culminate in cell death and the loss of neurons, which underlies much of the cognitive dysfunction that defines AD. Therefore, we were motivated to investigate whether the preservation of neuronal health seen in 5xFAD mice that lack STING was also associated with protection against neuronal cell death. To explore this possibility, we evaluated neuronal cell death in the CA1 region of the hippocampus in 5-month-old $5xSt^{KO}$ and 5xFAD mice by terminal deoxynucleotidyl transferase-mediated dUTP nick end labeling (TUNEL) assay. In line with our neuritic dystrophy and lipid peroxidation findings, we also observed reductions in TUNEL staining in the CA1 of STING-deficient 5xFAD mice in comparison to 5xFAD littermate controls (Figure 4G,H).

To investigate whether the improvements in neuronal health seen in 5xFAD mice that lack STING impact cognitive function, we next performed MWM testing to evaluate the ability of 4-month-old $5xSt^{KO}$ mice and 5xFAD littermate controls to learn and remember the location of a hidden platform based on visual cues and their aversion to water. We observed that in comparison to their 5xFAD littermates, $5xSt^{KO}$ mice were quicker to locate the hidden platform in its initial location (Figure 4I) and spent more time in the surrounding target quadrant after removal of the hidden platform (Figure 4J), indicating that they were better able to learn and recall spatial information. Taken together, these findings suggest that genetic ablation of STING in 5xFAD mice leads to improved neuronal health and protection against cognitive decline.

4 | DISCUSSION

In this study, we have uncovered a critical role for the innate immune signaling molecule STING in driving Aβ amyloidosis. More specifically, we find that genetic ablation of STING in the 5xFAD mouse model of AD-related amyloidosis leads to improved control of Aβ load, as well as protection against neuritic dystrophy and cognitive decline. snRNA-seq studies further revealed increased expression of neuronal health genes in excitatory neurons. Within microglia, we observed decreased expression of the disease-associated microglia (DAM) gene *Axl* as well as multiple genes involved in type I IFN-related signaling. Subsequent validation of our snRNA-seq data set confirmed that protection in 5xFAD $Sting1^{-/-}$ mice was associated with decreased staining of AXL and the key type I IFN-related signaling molecule STAT1 in IBA1+ microglia.

While mounting evidence clearly points to pivotal roles for the innate immune system in AD pathoetiology, it has become increasingly apparent that the overall effects of targeting most individual innate immune molecules are dependent on the stage of disease progression and the types of pathology present. For example, TREM2 deletion in Aβ amyloidosis models of AD has been extensively shown to cause exacerbated neurological disease,[47–54] whereas ablation of TREM2 in primary tauopathy models has been reported to limit neurodegenerative disease progression.[55–57] The divergent roles that many discrete innate molecules have been found to exert, which vary depending on the species of neuropathology present, have posed a challenge in the development of innate immune-targeting therapeutics for the treatment of AD. Despite this, STING and its related upstream sensor

---

0.05 and $\log_2$ fold changes ± 0.25. (E) Bar plots depicting upregulated GO terms enriched in 5xFAD microglia. Functional enrichment analysis was performed using g:Profiler using genes with adjusted *p*-values less than 0.05 and $\log_2$ fold changes ± 0.25. Depicted pathways were curated from the top driver terms in GO. (F–M) $5xSt^{KO}$ mice and 5xFAD littermate controls were harvested at 5 months of age to evaluate AXL and STAT1 expression by immunofluorescence staining. (F) Representative images of microglia (IBA1, blue), Aβ plaques (ThioS, red), and AXL (yellow; shown in inset) in the cortex (scale bar = 10 µm). White regions depict colocalization of AXL and IBA1 staining. (G) Number of AXL+ IBA1+ cells per FOV, (H) percentage of IBA1+ cells expressing AXL, and (I) number of AXL+ IBA1+ cells per plaque in the cortex ($n = 6$; 2 independent experiments). (J) Representative images of microglia (IBA1, blue) and STAT1 (yellow; shown in inset) in the cortex (scale bar = 15 µm). White regions denote colocalization of STAT1 and IBA1 staining. (K) Number of STAT1+ IBA1+ cells per FOV, (L) percentage of IBA1+ cells expressing STAT1+, and (M) number of STAT1+ IBA1+ cells per plaque in the cortex ($n = 8$; two independent experiments). Data points and error bars depict means per animal ± SEM, and statistical testing was performed by linear mixed-effects models (G–I) and (K–M). $^{*}p < 0.05$, $^{**}p < 0.01$, $^{***}p < 0.001$, $^{****}p < 0.0001$. Aβ, amyloid beta; AD, Alzheimer's disease; DEG, differentially expressed gene; FOV, field of view; GO, gene ontology; SEM, standard error of the mean; snRNA-seq, single-nuclei RNA sequencing; STING, stimulator of interferon genes; UMAP, uniform manifold approximation and projection.

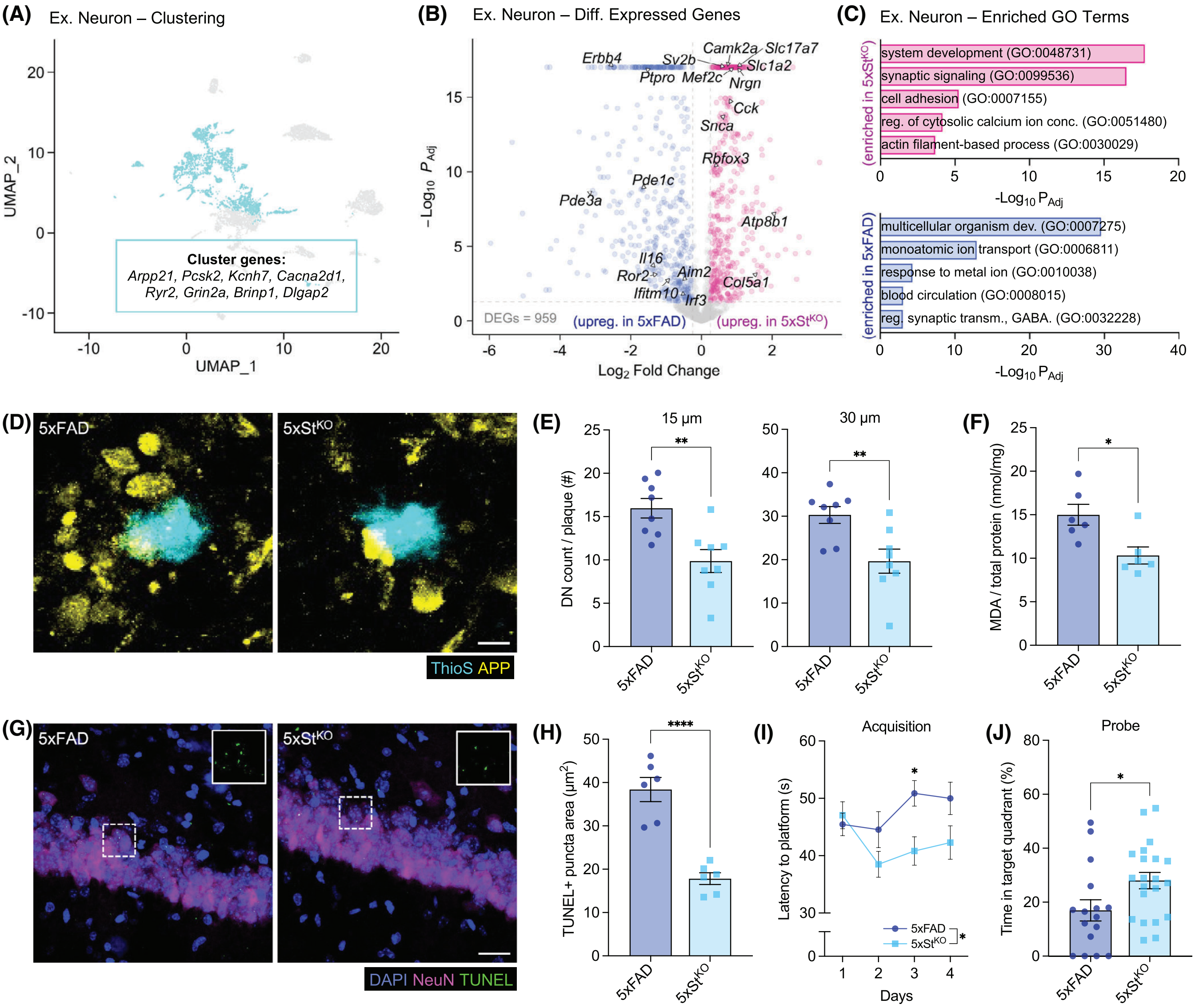

FIGURE 4 Genetic ablation of STING in 5xFAD mice leads to improvements in neuronal health and protection against cognitive decline. (A–C) The impact of STING deletion on neuronal gene expression was assessed in 6-month-old 5xFAD and 5xSt^{KO} mice by pooled snRNA-seq of cortical tissue ($n = 3$ per pooled sample). (A) UMAP plot depicting the excitatory neuron cluster. (B) Volcano plot depicting DEGs (upregulated, pink; downregulated, blue) in the excitatory neuron cluster of 5xSt^{KO} versus 5xFAD cortex. Colored points depict genes with adjusted p-values less than 0.05 and log$_2$ fold changes ± 0.25. (C) Bar plots depicting upregulated GO terms enriched in 5xSt^{KO} (top, pink) and 5xFAD (bottom, blue) excitatory neurons. Functional enrichment analysis was performed using g:Profiler using genes with adjusted p-values less than 0.05 and log$_2$ fold changes ± 0.25. Depicted pathways were curated from the top driver terms in GO. (D–I) 5xSt^{KO} mice and 5xFAD littermate controls were harvested at 5 months of age to evaluate neuritic dystrophy, oxidative stress, and neuronal cell death. (D) Representative images of DNs (APP, yellow) and Aβ plaques (ThioS, cyan) in the cortex (scale bar = 5 µm). (E) Enumeration of APP+ puncta DNs within 15 and 30 µm of Aβ plaques ($n = 7$–8; two independent experiments). (F) MDA concentration per total protein from whole-brain tissue lysates ($n = 6$ mice/group). (G) Representative images of cell death staining (TUNEL, green; shown in inset), neuronal nuclei (NeuN, magenta), and overall nuclei (DAPI, blue) in the CA1 region of the hippocampus (scale bar = 10 µm). (H) TUNEL percent area in the CA1. (I–J) MWM testing was conducted on 4-month-old 5xSt^{KO} mice and 5xFAD littermate controls to evaluate spatial learning and memory ($n = 15$ mice/group, four independent experiments). (I) Quantification of time spent to reach the platform during the acquisition phase and (J) time spent inside the target quadrant previously containing the old platform on a single MWM probe day. Statistical significance between experimental groups was calculated by linear mixed-effects models (E,F,H) and two-way ANOVA with Bonferroni's post-hoc test (I), and unpaired Student's t test (J). Data points in column graphs (E,F,H,J) represent individual mice, and data points in line graphs (I) represent means for each experimental group. All error bars represent mean ± SEM. $^{*}p < 0.05$, $^{**}p < 0.01$, $^{****}p < 0.0001$. Aβ, amyloid beta; ANOVA, analysis of variance; APP+, amyloid precursor protein positive; DEGs, differentially expressed gene; DNs, dystrophic neurites; FOV, field of view; GO, gene ontology; MDA, malondialdehyde; MWM, Morris water maze; SEM, standard error of the mean; snRNA-seq, single-nuclei RNA sequencing; STING, stimulator of interferon genes; TUNEL, terminal deoxynucleotidyl transferase-mediated dUTP nick end labeling; UMAP, uniform manifold approximation and projection.

molecule cGAS have emerged as attractive innate immune players to develop therapeutics around given the recent collective findings demonstrating that inhibiting this signaling axis provides protection against neurodegenerative disease progression in the context of either amyloidosis or tauopathy, as well as when both Aβ and tau pathology are present. Indeed, the earliest work on this topic showed that deletion of the STING-related DNA sensor cGAS in the P301S transgenic mouse model of tauopathy was effective in limiting cognitive decline and hippocampal synaptic loss.[17] More recent follow-up work from the same group further demonstrated that the expression of additional AD-associated risk genes such as *APOE4* and *TREM2-R47H* in female P301S mice leads to greater amplification of neurodegeneration and cGAS signaling,[58] which indicates that cGAS signaling may also contribute to AD progression in more complex genetic scenarios.

In terms of AD-associated amyloidosis, genetic ablation of cGAS was reported to provide protection in 5xFAD mice, which suggests that targeting cGAS inhibition in the early stages of disease when only Aβ is present could offer an effective treatment for AD. These findings are in line with the findings presented in this manuscript demonstrating that genetic ablation of the critical cGAS-related adaptor protein STING in 5xFAD mice results in protection against cognitive decline, reduced Aβ load, and improvement in neuronal health.[21] Of further translational significance, recently published studies have shown that treatment with the STING inhibitor H-151 limits the development of combined Aβ and tau pathology in App$^{\text{NL-G-F}}$/hTau double-knock-in mice[22]. However, it should be noted that future studies are also needed to test the therapeutic efficacy of other STING inhibitors in AD animal models, especially given that H-151 has been reported to have off-target effects.[23,24]

While these collective studies position the cGAS-STING signaling axis as a potentially promising innate immune pathway to target in the treatment of AD, numerous additional questions remain, which, once resolved, will lead to an improved understanding of cGAS-STING biology in neurodegenerative disease pathogenesis, and should also aid in the optimization of therapeutics targeting this pathway. For one, definitive in vivo studies have not yet been conducted to ascertain whether cGAS and STING influence AD-related pathogenesis through distinct or overlapping mechanisms. Although, STING signaling has been most extensively studied downstream of cytosolic DNA recognition and cGAS activation, emerging evidence indicates that aberrant vesicular trafficking, endoplasmic reticulum (ER) stress, and endolysosomal dysfunction can also incite STING activation independent of cGAS/DNA signaling.[59] This alternative mechanism of STING activation could be of potential relevance to AD, as defects in endolysosomal function and vesicular trafficking have been extensively linked to neuronal cell death and AD.[60] Most notably, mutations in numerous endolysosomal genes have been identified as genetic risk factors for AD.[7,60] Therefore, the potential exists that cGAS and STING might not have completely overlapping functions in neurodegeneration and this will be important to elucidate in future experiments.

It also remains to be determined in which specific cell types cGAS and STING function in to promote AD-related disease progression. This future area of investigation is of particular translational significance as cGAS and STING have been shown to be required to mount protective immune responses to multiple pathogens and cancer.[9–11] Therefore, cell-specific targeting of cGAS or STING may ultimately be needed to limit potential safety concerns associated with the global immunosuppression that occurs with systemic cGAS and STING inhibitor treatment. There is an ever-growing list of potential cell types, both in the brain and the periphery, that cGAS and STING could feasibly be acting in to drive AD pathogenesis. In the brain, emerging evidence suggests that cGAS and STING can coordinate immune responses in both microglia and neurons.[19,61–63] However, cGAS and STING could also potentially impact neurodegenerative disease pathogenesis through their regulation of peripheral immune cell infiltration into the brain. Of note, the role of peripheral-derived immune responses has been increasingly linked to AD pathogenesis.[64,65] For instance, T cells have emerged as pivotal players in multiple AD mouse models[66–68] and the cGAS-STING signaling axis has been shown to be a key regulator of T cell responses.[69–71] cGAS and STING could also potentially affect peripheral immune cell infiltration through their actions in endothelial cells.[72–74] For instance, dysregulated cGAS-STING signaling specifically endothelial cells was recently found to incite the infiltration of immune cells into the lung[74] and the potential exists that a similar phenomenon could be at play in the AD brain.

5 | CONCLUSION

In summary, these findings add to a growing body of literature implicating the innate immune adaptor protein STING as a major driver of neurodegenerative disease. Most notably, in addition to work by our group and others describing key roles for cGAS and STING in AD animal models, studies have also revealed pivotal roles for cGAS and/or STING in Parkinson's disease, amyotrophic lateral sclerosis, multiple sclerosis, and other age-related neurological diseases.[16–19,21,22,63,75] As such, continued efforts to develop specific therapeutics that target cGAS and STING could help to provide improved strategies to treat a wide range of neurodegenerative diseases.

AUTHOR CONTRIBUTIONS

Jessica M. Thanos, Nagaraj Kerur, and John R. Lukens designed the study; Jessica M. Thanos, Olivia C. Campbell, Nick R. Natale, Hannah E. Ennerfelt, Aman Mangalmurti, Katherine R. Bruch, and Katelyn A. Moore performed the experiments and analyzed the data; Maureen N. Cowan, Jessica M. Thanos, and Katherine R. Bruch performed the bioinformatics analyses; Katelyn A. Moore bred and maintained the animals; Jessica M. Thanos, Nagaraj Kerur, and John R. Lukens wrote the manuscript; Nagaraj Kerur and John R. Lukens oversaw the project.

ACKNOWLEDGMENTS

We thank members of the Lukens Lab and the Center for Brain Immunology and Glia (BIG) at the University of Virginia for valuable discussions. This work was supported by The National Institutes of Health/National Institute of Aging (R01AG071996, R01AG087406, and RF1AG078684; awarded to J.R.L.), The Alzheimer's Association

(ADSF-21-816651; awarded to J.R.L.), the Cure Alzheimer's Fund (awarded to J.R.L.), The Owens Family Foundation (Awarded to J.R.L.), and The Harrison Family Foundation (awarded to J.R.L.). J.M.T. was supported by the Brain Immunology and Glia Training Program Grant (T32NS115657). O.C. was supported by a Harrison Undergraduate Research Award.

CONFLICT OF INTEREST STATEMENT

The authors declare no conflicts of interest. Author disclosures are available in the Supporting Information.

CONSENT STATEMENT

This work did not involve the use of material from human subjects.

ORCID

Jessica M. Thanos https://orcid.org/0000-0001-7984-5361
John R. Lukens https://orcid.org/0000-0002-6795-0866

REFERENCES

1. Heneka MT, van der Flier WM, Jessen F, et al. Neuroinflammation in Alzheimer disease. *Nat Rev Immunol*. 2025;25:321-352.
2. Chen X, Holtzman DM. Emerging roles of innate and adaptive immunity in Alzheimer's disease. *Immunity*. 2022;55:2236-2254.
3. Ennerfelt HE, Lukens JR. The role of innate immunity in Alzheimer's disease. *Immunol Rev*. 2020;297:225-246.
4. Johnson AM, Lukens JR. The innate immune response in tauopathies. *Eur J Immunol*. 2023;53:e2250266.
5. Samuels JD, Lukens JR, Price RJ. Emerging roles for ITAM and ITIM receptor signaling in microglial biology and Alzheimer's disease-related amyloidosis. *J Neurochem*. 2024;168:3558-3573.
6. Efthymiou AG, Goate AM. Late onset Alzheimer's disease genetics implicates microglial pathways in disease risk. *Mol Neurodegener*. 2017;12:43.
7. Podlesny-Drabiniok A, Marcora E, Goate AM. Microglial phagocytosis: a disease-associated process emerging from Alzheimer's disease genetics. *Trends Neurosci*. 2020;43:965-979.
8. Karch CM, Goate AM. Alzheimer's disease risk genes and mechanisms of disease pathogenesis. *Biol Psychiatry*. 2015;77:43-51.
9. Decout A, Katz JD, Venkatraman S, Ablasser A. The cGAS-STING pathway as a therapeutic target in inflammatory diseases. *Nat Rev Immunol*. 2021;21:548-569.
10. Yang K, Tang Z, Xing C, Yan N. STING signaling in the brain: molecular threats, signaling activities, and therapeutic challenges. *Neuron*. 2024;112:539-557.
11. Ablasser A, Chen ZJ. cGAS in action: expanding roles in immunity and inflammation. *Science*. 2019;363:eaat8657.
12. Ishikawa H, Barber GN. STING is an endoplasmic reticulum adaptor that facilitates innate immune signalling. *Nature*. 2008;455:674-678.
13. Ablasser A, Goldeck M, Cavlar T, et al. cGAS produces a 2'-5'-linked cyclic dinucleotide second messenger that activates STING. *Nature*. 2013;498:380-384.
14. Civril F, Deimling T, de Oliveira Mann CC, et al. Structural mechanism of cytosolic DNA sensing by cGAS. *Nature*. 2013;498:332-337.
15. Burdette DL, Monroe KM, Sotelo-Troha K, et al. STING is a direct innate immune sensor of cyclic di-GMP. *Nature*. 2011;478:515-518.
16. Yu CH, Davidson S, Harapas CR, et al. TDP-43 triggers mitochondrial DNA release via mPTP to activate cGAS/STING in ALS. *Cell*. 2020;183:636-649.
17. Udeochu JC, Amin S, Huang Y, et al. Tau activation of microglial cGAS-IFN reduces MEF2C-mediated cognitive resilience. *Nat Neurosci*. 2023;26:737-750.
18. Hinkle JT, Patel J, Panicker N, et al. STING mediates neurodegeneration and neuroinflammation in nigrostriatal alpha-synucleinopathy. *Proc Natl Acad Sci U S A*. 2022;119:e2118819119.
19. Gulen MF, Samson N, Keller A, et al. cGAS-STING drives ageing-related inflammation and neurodegeneration. *Nature*. 2023;620:374-380.
20. Huang Y, Liu B, Sinha SC, Amin S, Gan L. Mechanism and therapeutic potential of targeting cGAS-STING signaling in neurological disorders. *Mol Neurodegener*. 2023;18:79.
21. Xie X, Ma G, Li X, Zhao J, Zhao Z, Zeng J. Activation of innate immune cGAS-STING pathway contributes to Alzheimer's pathogenesis in 5xFAD mice. *Nat Aging*. 2023;3:202-212.
22. Chung S, Jeong JH, Park JC, et al. Blockade of STING activation alleviates microglial dysfunction and a broad spectrum of Alzheimer's disease pathologies. *Exp Mol Med*. 2024;56:1936-1951.
23. Barasa L, Chaudhuri S, Zhou JY, et al. Development of LB244, an irreversible STING antagonist. *J Am Chem Soc*. 2023;145:20273-20288.
24. Hong Z, Mei J, Li C, et al. STING inhibitors target the cyclic dinucleotide binding pocket. *Proc Natl Acad Sci U S A*. 2021;118:e2105465118.
25. Oakley H, Cole SL, Logan S, et al. Intraneuronal beta-amyloid aggregates, neurodegeneration, and neuron loss in transgenic mice with five familial Alzheimer's disease mutations: potential factors in amyloid plaque formation. *J Neurosci*. 2006;26:10129-10140.
26. Jin L, Hill KK, Filak H. MPYS is required for IFN response factor 3 activation and type I IFN production in the response of cultured phagocytes to bacterial second messengers cyclic-di-AMP and cyclic-di-GMP. *J Immunol*. 2011;187:2595-2601.
27. Da Mesquita S, Louveau A, Vaccari A, et al. Functional aspects of meningeal lymphatics in ageing and Alzheimer's disease. *Nature*. 2018;560:185-191.
28. Wolf FA, Angerer P, Theis FJ. SCANPY: large-scale single-cell gene expression data analysis. *Genome Biol*. 2018;19:15.
29. Wolock SL, Lopez R, Klein AM. Scrublet: computational identification of cell doublets in single-cell transcriptomic data. *Cell Syst*. 2019;8:281-291.
30. Bernstein NJ, Fong NL, Lam I, Roy MA, Hendrickson DG, Kelley DR. Solo: doublet identification in single-cell RNA-Seq via semi-supervised deep learning. *Cell Syst*. 2020;11:95-101.
31. Gayoso A, Lopez R, Xing G, et al. A Python library for probabilistic analysis of single-cell omics data. *Nat Biotechnol*. 2022;40:163-166.
32. Eraslan G, Drokhlyansky E, Anand S, et al. Single-nucleus cross-tissue molecular reference maps toward understanding disease gene function. *Science*. 2022;376:eabl4290.
33. Caglayan E, Liu Y, Konopka G. Neuronal ambient RNA contamination causes misinterpreted and masked cell types in brain single-nuclei datasets. *Neuron*. 2022;110:4043-4056.
34. Ferecsko AS, Smallwood MJ, Moore A, et al. STING-triggered CNS inflammation in human neurodegenerative diseases. *Biomedicines*. 2023;11.
35. Suberbielle E, Sanchez PE, Kravitz AV, et al. Physiologic brain activity causes DNA double-strand breaks in neurons, with exacerbation by amyloid-beta. *Nat Neurosci*. 2013;16:613-621.
36. Shanbhag NM, Evans MD, Mao W, et al. Early neuronal accumulation of DNA double strand breaks in Alzheimer's disease. *Acta Neuropathol Commun*. 2019;7:77.
37. Ren J, Zhang S, Wang X, et al. MEF2C ameliorates learning, memory, and molecular pathological changes in Alzheimer's disease in vivo and in vitro. *Acta Biochim Biophys Sin*. 2022;54:77-90.
38. Deczkowska A, Matcovitch-Natan O, Tsitsou-Kampeli A, et al. Mef2C restrains microglial inflammatory response and is lost in brain ageing in an IFN-I-dependent manner. *Nat Commun*. 2017;8:717.

39. Woo RS, Lee JH, Yu HN, Song DY, Baik TK. Expression of ErbB4 in the neurons of Alzheimer's disease brain and APP/PS1 mice, a model of Alzheimer's disease. *Anat Cell Biol*. 2011;44:116-127.
40. Lee HJ, Jung KM, Huang YZ, et al. Presenilin-dependent gamma-secretase-like intramembrane cleavage of ErbB4. *J Biol Chem*. 2002;277:6318-6323.
41. Zhang H, Zhang L, Zhou D, et al. Ablating ErbB4 in PV neurons attenuates synaptic and cognitive deficits in an animal model of Alzheimer's disease. *Neurobiol Dis*. 2017;106:171-180.
42. Zhang H, Zhang L, Zhou D, Li H, Xu Y. ErbB4 mediates amyloid beta-induced neurotoxicity through JNK/tau pathway activation: implications for Alzheimer's disease. *J Comp Neurol*. 2021;529:3497-3512.
43. Montine TJ, Neely MD, Quinn JF, et al. Lipid peroxidation in aging brain and Alzheimer's disease. *Free Radic Biol Med*. 2002;33:620-626.
44. Garcia-Alloza M, Dodwell SA, Meyer-Luehmann M, Hyman BT, Bacskai BJ. Plaque-derived oxidative stress mediates distorted neurite trajectories in the Alzheimer mouse model. *J Neuropathol Exp Neurol*. 2006;65:1082-1089.
45. Ferre-Gonzalez L, Pena-Bautista C, Baquero M, Chafer-Pericas C. Assessment of lipid peroxidation in Alzheimer's disease differential diagnosis and prognosis. *Antioxidants (Basel)*. 2022;11:551.
46. Lopez N, Tormo C, De Blas I, Llinares I, Alom J. Oxidative stress in Alzheimer's disease and mild cognitive impairment with high sensitivity and specificity. *J Alzheimers Dis*. 2013;33:823-829.
47. Zhao Y, Wu X, Li X, et al. TREM2 is a receptor for beta-amyloid that mediates microglial function. *Neuron*. 2018;97:1023-1031.
48. Jay TR, Hirsch AM, Broihier ML, et al. Disease progression-dependent effects of TREM2 deficiency in a mouse model of Alzheimer's disease. *J Neurosci*. 2017;37:637-647.
49. Cheng-Hathaway PJ, Reed-Geaghan EG, Jay TR, et al. The Trem2 R47H variant confers loss-of-function-like phenotypes in Alzheimer's disease. *Mol Neurodegener*. 2018;13:29.
50. Ulland TK, Song WM, Huang SC, et al. TREM2 maintains microglial metabolic fitness in Alzheimer's disease. *Cell*. 2017;170:649-663.e13.
51. Wang Y, Cella M, Mallinson K, et al. TREM2 lipid sensing sustains the microglial response in an Alzheimer's disease model. *Cell*. 2015;160:1061-1071.
52. Wang Y, Ulland TK, Ulrich JD, et al. TREM2-mediated early microglial response limits diffusion and toxicity of amyloid plaques. *J Exp Med*. 2016;213:667-675.
53. Yuan P, Condello C, Keene CD, et al. TREM2 Haplodeficiency in mice and humans impairs the microglia barrier function leading to decreased amyloid compaction and severe axonal dystrophy. *Neuron*. 2016;92:252-264.
54. Song WM, Joshita S, Zhou Y, Ulland TK, Gilfillan S, Colonna M. Humanized TREM2 mice reveal microglia-intrinsic and -extrinsic effects of R47H polymorphism. *J Exp Med*. 2018;215:745-760.
55. Leyns CEG, Gratuze M, Narasimhan S, et al. TREM2 function impedes tau seeding in neuritic plaques. *Nat Neurosci*. 2019;22:1217-1222.
56. Leyns CEG, Ulrich JD, Finn MB, et al. TREM2 deficiency attenuates neuroinflammation and protects against neurodegeneration in a mouse model of tauopathy. *Proc Natl Acad Sci U S A*. 2017;114:11524-11529.
57. Sayed FA, Telpoukhovskaia M, Kodama L, et al. Differential effects of partial and complete loss of TREM2 on microglial injury response and tauopathy. *Proc Natl Acad Sci U S A*. 2018;115:10172-10177.
58. Carling GK, Fan L, Foxe NR, et al. Alzheimer's disease-linked risk alleles elevate microglial cGAS-associated senescence and neurodegeneration in a tauopathy model. *Neuron*. 2024;112:3877-3896.
59. Jeltema D, Abbott K, Yan N. STING trafficking as a new dimension of immune signaling. *J Exp Med*. 2023;220:e20220990.
60. Szabo MP, Mishra S, Knupp A, Young JE. The role of Alzheimer's disease risk genes in endolysosomal pathways. *Neurobiol Dis*. 2022;162:105576.
61. Liu Y, Wang A, Chen C, et al. Microglial cGAS-STING signaling underlies glaucoma pathogenesis. *Proc Natl Acad Sci U S A*. 2024;121:e2409493121.
62. Marques C, Held A, Dorfman K, et al. Neuronal STING activation in amyotrophic lateral sclerosis and frontotemporal dementia. *Acta Neuropathol*. 2024;147:56.
63. Woo MS, Mayer C, Binkle-Ladisch L, et al. STING orchestrates the neuronal inflammatory stress response in multiple sclerosis. *Cell*. 2024;187:4043-4060.
64. Gate D, Saligrama N, Leventhal O, et al. Clonally expanded CD8 T cells patrol the cerebrospinal fluid in Alzheimer's disease. *Nature*. 2020;577:399-404.
65. Jorfi M, Park J, Hall CK, et al. Infiltrating CD8(+) T cells exacerbate Alzheimer's disease pathology in a 3D human neuroimmune axis model. *Nat Neurosci*. 2023;26:1489-1504.
66. Machhi J, Yeapuri P, Lu Y, et al. CD4+ effector T cells accelerate Alzheimer's disease in mice. *J Neuroinflammation*. 2021;18:272.
67. Chen X, Firulyova M, Manis M, et al. Microglia-mediated T cell infiltration drives neurodegeneration in tauopathy. *Nature*. 2023;615:668-677.
68. Su W, Saravia J, Risch I, et al. CXCR6 orchestrates brain CD8(+) T cell residency and limits mouse Alzheimer's disease pathology. *Nat Immunol*. 2023;24:1735-1747.
69. Larkin B, Ilyukha V, Sorokin M, Buzdin A, Vannier E, Poltorak A. Cutting edge: activation of STING in T cells induces type I IFN responses and cell death. *J Immunol*. 2017;199:397-402.
70. Li W, Lu L, Lu J, et al. cGAS-STING-mediated DNA sensing maintains CD8(+) T cell stemness and promotes antitumor T cell therapy. *Sci Transl Med*. 2020;12:eaay9013.
71. Wu J, Chen YJ, Dobbs N, et al. STING-mediated disruption of calcium homeostasis chronically activates ER stress and primes T cell death. *J Exp Med*. 2019;216:867-883.
72. Pais TF, Ali H, Moreira da Silva J, et al. Brain endothelial STING1 activation by Plasmodium-sequestered heme promotes cerebral malaria via type I IFN response. *Proc Natl Acad Sci U S A*. 2022;119:e2206327119.
73. Liu H, Ghosh S, Vaidya T, et al. Activated cGAS/STING signaling elicits endothelial cell senescence in early diabetic retinopathy. *JCI Insight*. 2023;8:e168945.
74. Gao KM, Chiang K, Jiang Z, et al. Endothelial cell expression of a STING gain-of-function mutation initiates pulmonary lymphocytic infiltration. *Cell Rep*. 2024;43:114114.
75. Wang A, Chen C, Mei C, et al. Innate immune sensing of lysosomal dysfunction drives multiple lysosomal storage disorders. *Nat Cell Biol*. 2024;26:219-234.

SUPPORTING INFORMATION

Additional supporting information can be found online in the Supporting Information section at the end of this article.

How to cite this article: Thanos JM, Campbell OC, Cowan MN, et al. STING deletion protects against amyloid β–induced Alzheimer's disease pathogenesis. *Alzheimer's Dement*. 2025;21:e70305. https://doi.org/10.1002/alz.70305